Planktonic foraminifera, sea surface temperatures, and mechanisms of oceanic change in the Peru and south equatorial currents, 0–150 ka BP

Melissa J. Feldberg and Alan C. Mix

College of Oceanic and Atmospheric Sciences, Oregon State University, Corvallis, Oregon, USA

Received 16 November 2001; revised 19 July 2002; accepted 5 September 2002; published 25 March 2003.

[1] Planktonic foraminiferal faunas of the southeast Pacific indicate that sea surface temperatures (SST) have varied by as much as 8–10°C in the Peru Current, and by ~5–7°C along the equator, over the past 150,000 years. Changes in SST at times such as the Last Glacial Maximum reflect incursion of high-latitude species *Globorotalia inflata* and *Neogloboquadrina pachyderma* into the eastern boundary current and as far north as the equator. A simple heat budget model of the equatorial Pacific shows that observed changes in Peru Current advection can account for about half of the total variability in equatorial SSTs. The remaining changes in equatorial SST, which are likely related to local changes in upwelling or pycnocline depth, precede changes in polar climates as recorded by $\delta^{18}O$. This partitioning of processes in eastern equatorial Pacific SST reveals that net ice-age cooling here reflects first a rapid response of equatorial upwelling to insolation, followed by a later response to changes in the eastern boundary current associated with high-latitude climate (which closely resembles variations in atmospheric CO_2 as recorded in the Vostok ice core). Although precise mechanisms responsible for the equatorial upwelling component of climate change remain uncertain, one likely candidate that may operate independently of the ice sheets is insolation-driven changes in El Niño/Southern Oscillation (ENSO) frequency. Early responses of equatorial SST detected both here and elsewhere highlight the sensitivity of tropical systems to small changes in seasonal insolation. The scale of tropical changes we have observed are substantially greater than model predictions, suggesting a need for further quantitative assessment of processes associated with long-term climate change. *INDEX TERMS:* 3030 Marine Geology and Geophysics: Micropaleontology; 4267 Oceanography: General: Paleoceanography; 4516 Oceanography: Physical: Eastern boundary currents; 9355 Information Related to Geographic Region: Pacific Ocean; *KEYWORDS:* paleoceanography, Pacific Ocean, eastern boundary current, foraminifera, sea surface temperature

Citation: Feldberg, M. J., and A. C. Mix, Planktonic foraminifera, sea surface temperatures, and mechanisms of oceanic change in the Peru and south equatorial currents, 0–150 ka BP, *Paleoceanography*, *18*(1), 1016, doi:10.1029/2001PA000740, 2003.

1. Introduction

[2] Recent estimates of paleotemperature indicate that the eastern tropical Pacific Ocean has been more sensitive to global climate change over the last glacial cycle (0–150,000 years) than previously thought [*Patrick and Thunell*, 1997; *Pisias and Mix*, 1997; *Mix et al.*, 1999; *Crowley*, 2000; *Lea et al.*, 2000]. Previous temperature reconstructions of the southeast Pacific have been severely limited by a paucity of dated sediment cores [*CLIMAP*, 1981]. With new sediment cores for the region to facilitate better regional calibration of SST estimates, *Feldberg and Mix* [2002] suggested that SSTs of the Last Glacial Maximum (LGM) off Southern Peru were much cooler than at present, and that changes here were even larger than along the equator [*Mix et al.*, 1999]. A simple heat budget model suggested that advection of cool water off the eastern boundary of South America could account for much of the observed LGM cooling of the equatorial Pacific cold tongue.

[3] Here we assess variations in the Peru Current and its influence on the eastern equatorial Pacific in time series over the last glacial cycle (0–150 ka). Is this current consistently stronger during glacial maxima, or is this phenomenon unique to the LGM? Are SST changes in the eastern boundary current synchronous with changes in the equatorial Pacific? Can we isolate the effects of eastern boundary current advection from local wind-driven upwelling on SST in the equatorial cold tongue? Do temporal patterns of change reveal mechanisms responsible for changing climate? To address these questions, we examine changes in foraminiferal faunas and estimate SST over the past 150,000 years in four sediment cores under the eastern boundary current and the equatorial Pacific. We examine possible processes responsible for the large temperature variations observed in the Peru Current, and assess the effect of changes in the strength and temperature of this current on the equatorial Pacific by extending the heat budget model of *Feldberg and Mix* [2002] to examine linkages between these two areas.

2. Study Sites and Regional Oceanography

[4] To assess variations in the eastern boundary current, we examine three sediment cores located on the flanks of the Nazca Ridge, an aseismic ridge off the coast of Peru.

0883-8305/03/2001PA000740$12.00

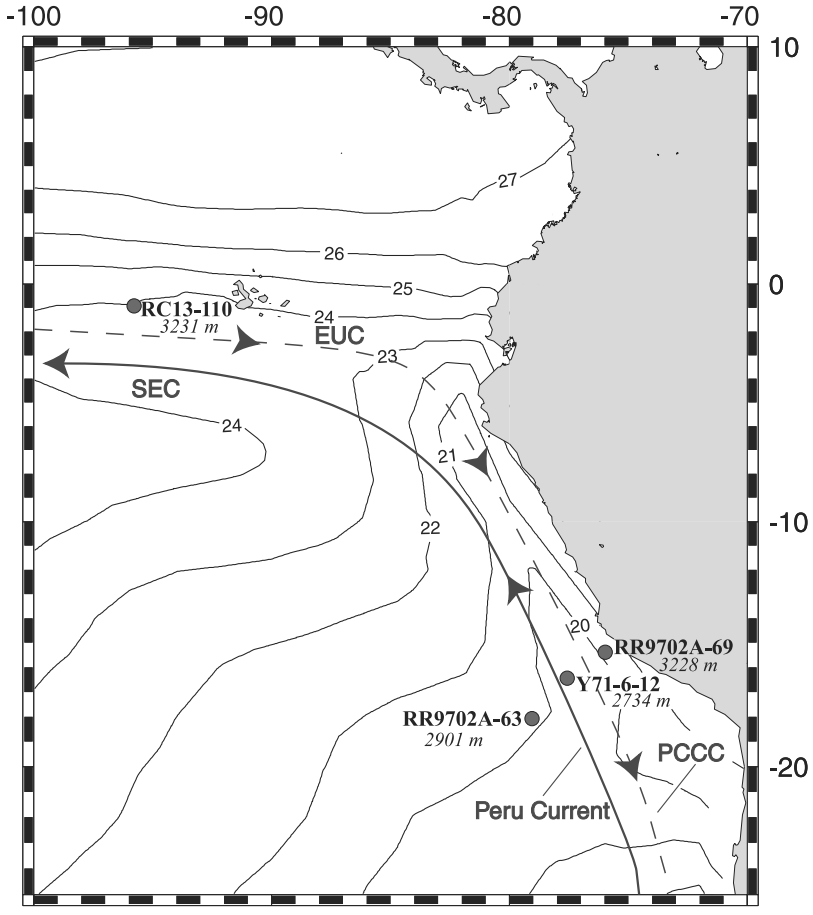

Figure 1. Location of the cores used in this study (circles). Major surface currents (solid lines) affecting SST at these sites are the Peru Current and the South Equatorial Current (SEC), and the Peru-Chile Countercurrent (PCCC). Subsurface currents (dashed lines) are the Equatorial Undercurrent (EUC, 200–250 m depth, near the equator) and the Peru-Chile Undercurrent (PCU, 50–150 m depth) (schematic after *Strub et al.* [1998]). Contours are of annual average SST in °C [*Ocean Climate Laboratory*, 1999].

These cores form a transect across the overlying Peru Current (Figure 1). Core RR9702A-69TC (trigger core, hereafter 69TC) (16.007°S, 76.328°W, 3228 m depth) is located 150 km offshore. Modern annual-average SST at 69TC is 19.6°C based on the World Ocean Atlas 1998 [*Ocean Climate Laboratory*, 1999] (hereafter referred to as WOA98). Core Y71-6-12 (16.443°S, 77.563°W, 2734 m depth) is located 250 km from the coast. Modern annual-average SST here is 19.8°C (WOA98). The site of core RR9702A-63TC (hereafter 63TC) (18.085°S, 79.040°W, 2901 m depth, approximately 520 km offshore) presently has an average annual temperature of 21.1°C (WOA98).

[5] To estimate SST in these cores, we apply the "downcore + coretop" calibration equation for planktonic foraminifera derived by *Feldberg and Mix* [2002]. This equation is based on that of *Imbrie and Kipp* [1971] but includes new core-top calibration samples from the southeast Pacific and downcore samples in the definition of faunal factors, following *Mix et al.* [1999].

[6] As a representative site for the equatorial cold tongue in the eastern Pacific, we use core RC13-110 (0.097°S, 95.653°W, 3231 m depth). Here the modern annual-average SST is 23.8°C (WOA98). At this site, we estimate variations in SST using the foraminiferal transfer function of *Mix et al.* [1999], which was optimized for equatorial conditions while avoiding modern analog problems. These results for RC13-110 are remarkably similar in both amplitude and temporal variability to temperature estimates at nearby core TR163-19 based on Mg/Ca in planktonic foraminifera [*Lea et al.*, 2000].

[7] Much of the cool water along the eastern boundary originates at high southern latitudes and is advected northward in the Peru Current, a broad, slow current with an average transport of 15–20 Sv (1 Sv = 10^6 m^3s^{-1}) [*Wooster and Reid*, 1963]. The Peru Current flows northwestward over the Nazca Ridge with a velocity of 0–10 cm/s in the upper 100 m of the water column [*Huyer et al.*, 1991]. At depths >100 m, poleward flows associated with the Peru-Chile Undercurrent are dominant [*Strub et al.*, 1998]. Near the shelf-slope break, relatively warm low-latitude water is advected southward in the Peru-Chile Countercurrent [*Strub et al.*, 1995].

[8] Along the coast of Peru and Chile, cold (11–14°C) and nutrient-rich subsurface waters upwell [*Strub et al.*,

1998]. Some of this water transits from the southwest Pacific in the lower portions of the equatorial undercurrent and then back southward along the coast of South America in the Peru-Chile Undercurrent before reaching the surface [*Toggweiler et al.*, 1991]. Coastal upwelling is generally limited to within 50–60 km of the shoreline [*Strub et al.*, 1998].

[9] Our study sites are outside of the active coastal upwelling centers, and thus reflect conditions of the open-ocean Peru Current. Core 69TC may be influenced by offshore mixing of cool waters upwelled along the coast as well as warmer waters advected southward in the Peru-Chile Countercurrent, and core 63TC is influenced by mixing with warmer waters of the subtropical gyre. Core Y71-6-12 is near the present core of the Peru Current. We selected these three sites specifically to span the full range of conditions within the Peru Current, so that by averaging the records we can approximate the integrated character of the watermass advected equatorward, independent of small shifts in the position of the currents over time.

[10] Near 5°S, the cool Peru Current is deflected away from the coast. Here water from the eastern boundary enters the South Equatorial Current, which flows westward as the equatorial cool tongue between approximately 4°N and 10°S latitude [*Wyrtki*, 1965]. The cool tongue is maintained to the west by active upwelling along the equatorial divergence from a relatively shallow thermocline [*Wyrtki*, 1981; *Bryden and Brady*, 1985].

3. Materials and Taxonomic Data

[11] Cores 69TC, Y71-6-12, and 63TC were sampled for planktonic foraminifera at approximately 4000-year intervals over the past 150,000 years, taking into account the different sedimentation rates of each core. Some intervals in 69TC were barren of planktonic foraminifera. The sediment samples were freeze-dried, weighed, and washed through a 63 μm sieve using a 0.5% sodium hexa-meta-phosphate cleaning solution and rinsed with distilled water. The remaining >63 μm fraction of each sample was oven-dried, weighed, and split into two equal fractions, one to be used for planktonic foraminifera species counts and one reserved for stable isotope analysis and radiocarbon dating.

[12] The sample fraction used for foraminifera species counts was dry sieved at 150 μm and divided using a microsplitter until the sample contained approximately 350 foraminifera. All planktonic foraminifera in the sample split were identified and counted at the species level using the taxonomy of *Parker* [1962]. Species counts were converted to percentages with closure around twenty-six species [*Feldberg and Mix*, 2002]. Raw species counts are available at the US National Geologic Data Center (http://www.ngdc.noaa.gov/paleo/paleo.html).

4. Stratigraphy and Chronology

4.1. Stable Isotope Data

[13] Isotopic analyses of $\delta^{18}O$ and $\delta^{13}C$ in the benthic foraminifera *Uvigerina peregrina* and *Cibicides wuellerstorfi* from cores 69TC, Y71-6-12, and 63TC included approximately six individual foraminifera of each species in the size fraction >150 μm. The samples were cleaned ultrasonically in deionized water, dried, and roasted for 1 hour at 400°C under high vacuum. Isotopic measurements were made using a Finnigan/MAT251 mass spectrometer coupled to an Autoprep Systems carbonate reaction device at Oregon State University. The carbonate reactions occurred under vacuum in ~100% orthophosphoric acid at 90°C. Isotope data and time scales in RC13-110 were published previously [*Mix et al.*, 1991].

[14] The isotope data are reported using the standard delta (δ) notation in per mil (‰) relative to Pee Dee Belemnite (PDB) using the NBS-19 and NBS-20 standards. External precision estimates based on replicate analysis of local standards are ±0.06‰ for $\delta^{18}O$ and ±0.03‰ for $\delta^{13}C$. All stable isotope data are available from NGDC. The raw $\delta^{18}O$ values from *Cibicides wuellerstorfi* were increased by 0.64 to correct for a well-known species offset and averaged with data from *Uvigerina peregrina* at the same depth to produce a single $\delta^{18}O$ curve for each core.

4.2. Biostratigraphy

[15] Within the Peru Current off southern Peru, we found the relative abundances of the species *Globorotalia inflata* and *Pulleniatina obliquiloculata* to be useful biostratigraphic markers to augment correlations based on $\delta^{18}O$. *G. inflata* is common in the Peru Current during cool (roughly glacial) intervals and rare or absent during warm (roughly interglacial) intervals. In contrast, *P. obliquiloculata* is abundant during warm intervals, and rare or absent during cool intervals. Peaks in *G. inflata* abundance are common in the southeast Pacific; for example, an event associated with the LGM (21,000 calendar years) appears to extend northward to cores ODP846 [*Le et al.*, 1995] near Galapagos, and RC13-110 on the equator. This biostratigraphic pattern helped to correlate cores 63TC and 69TC to Y71-6-12, where the isotopic stratigraphy was best developed. Although it is possible that the faunal variations at these three sites are not perfectly synchronous, it is reasonable to expect that similar species variations would occur at roughly the same time in 63TC and 69TC as in Y71-6-12, due to the proximity of these sites.

4.3. Radiocarbon Dates

[16] Radiocarbon dates used approximately 7 mg of mixed species of benthic foraminifera in each sample. These samples were chosen at or bracketing the approximate depths of the LGM based on the stable isotope stratigraphy (30–32 cm and 70–72 cm in RR9702A-69TC, 44–47 cm in Y71-6-12, and 16–17cm in core RR9702A-63TC). All ^{14}C analyses were made at the National Ocean Science Accelerator Mass Spectrometer (NOSAMS) Facility at Woods Hole Oceanographic Institution. The modern deep-water ^{14}C reservoir age at the sites is 2100 years (1700 years older than surface waters) [*Toggweiler et al.*, 1989]. Calendar ages, calculated using the CALIB 4.2 software with the marine calibration data set [*Stuiver and Reimer*, 1993; *Stuiver et al.*, 1998] are reported in Table 1.

4.4. Age Models

[17] After developing stratigraphic ties among cores 69TC, Y71-6-12, and 63TC using both isotopic and faunal

Table 1. Radiocarbon Ages for Cores Used in This Study Including Raw AMS Age, Analytical Error, Reservoir-Corrected Age, and Calendar Age

Core	Depth, cm	^{14}C Raw Age, yBP	^{14}C Error, years, 1σ	Reservoir Corrected ^{14}C Age, yBP[a]	Calendar Age, yBP
69TC	30–32	12700	65	10600	12472
69TC	70–72	18850	85	16750	19839
63TC	16–17	20900	140	18800	22198
Y71-6-12	44–47	17500	95	15400	18285

[a]Reservoir ages are raw ages minus 2100 years, 400 years of which is a time-dependent global ocean reservoir correction [*Stuiver and Reimer*, 1993]. The remaining 1700 years is the local reservoir correction for the deep southeastern Pacific [*Toggweiler et al.*, 1989].

data, we constructed age models primarily from visual correlation of the benthic foraminiferal δ^{18}O records of these cores to the isotope chronology of core V19-30 (3.35°S, 83.35°W, 3091 m depth) [*Shackleton and Pisias*, 1985]. Although a recent modification to this age model [*Shackleton*, 2000] would increase ages slightly, we use the original age model for V19-30 because it is consistent with that of SPECMAP [*Imbrie et al.*, 1984] and thus facilitates comparisons with many other records, including RC13-110. Nevertheless, we recognize that the SPECMAP timescale includes some uncertainties. Thus, although our primary age model remains consistent with that of SPECMAP, in the discussion we allow for a possible modification of this age model based on U-Th dates which suggest an age of ~135 ka for the MIS 5/6 boundary, roughly 5% older than SPECMAP [*Henderson and Slowey*, 2000]. For the Nazca Ridge cores, we assigned ages to peaks and major transitions in the δ^{18}O records, and included calendar-corrected radiocarbon ages in each core as control points for creating the age models (Table 2). We determined the ages of all samples between control points using linear interpolation.

[18] The δ^{18}O record of core Y71-6-12 displays a familiar glacial-interglacial pattern, similar to that of V19-30 (Figure 2). The maximum error of this age model relative to the standard model is ~4 kyr. Time shifts of more than this amount in either direction would result in a clear mismatch of these records. The average sedimentation rate in core Y71-6-12 is 1.6 cm/kyr.

[19] The isotope record of 63TC is less diagnostic than that of Y71-6-12. For example, the δ^{18}O record of the transition from MIS 5 to 6 (Termination II) is unusually long and chaotic in 63TC. This is due to the low average sedimentation rate of this core, 0.6 cm/kyr, coupled to the effects of bioturbation. Benthic foraminifera are rare at this site, and this exacerbates the effect of any bioturbation on the δ^{18}O reconstruction because mixing of relatively rare benthic foraminifera that carry the isotope signal into a zone that would otherwise be barren of the appropriate benthic species can result in a confused isotopic stratigraphy. Although bioturbation also influences planktic foraminiferal abundances, the effect is less damaging for simple abundances than for compound signals of variable tracers carried on rare particles of varying abundance, which is known as the "bioturbation-abundance couple" [*Broecker et al.*, 1984; *Mix and Ruddiman*, 1985]. We retain core 63TC in our analysis because its position >500 km offshore provides for a full transect of the Peru Current, and rely mostly on its biostratigraphic links to the core Y71-6-12 to establish its chronology (Table 2). In addition, we use the radiocarbon date at 22.6 ka (calendar age) and the assumption that the top of the core contains modern sediments to establish the chronology for the upper part of the record. Applying this age model to the species data results in reasonable correlations between the cores for the most abundant species (Figure 3), and does not violate the isotope data (Figure 2).

[20] The age model for core 69TC was produced in a similar manner to that of 63TC. We used two radiocarbon dates as control points in the upper section of the core and isotope and faunal correlation in the deeper sections. The age model is well constrained at ages younger than 75 ka with an estimated error of ±4 kyr. Beyond this age, the core is essentially barren of foraminifera. For this reason, we will limit our discussion of this core to the last 75,000 years. The average sedimentation rate in this interval of core 69TC is 3.4 cm/kyr.

5. Foraminiferal Faunas and Sea Surface Temperatures

5.1. Factor Analysis

[21] Q-mode factor analysis was performed on species data from coretop and downcore samples in the eastern Pacific (140°W to 70°W longitude, 50°N to 50°S latitude)

Table 2. Depth-Age Pairs Used As Control Points for Constructing the Age Models of Cores Y71-6-12, RR9702A-69TC and RR9702A-63TC[a]

Y71-6-12		RR9702A-69TC		RR9702A-63TC	
Depth, cm	Age, ky	Depth, cm	Age, ky	Depth, cm	Age, ky
0	0.0	0	0.0	0	0.0
		16	3.5	17	22.2
30	12.5	31	12.5	42	70.0
		45	14.0	52	85.0
46	18.3	71	19.8	88	130.0
130	74.0	291	80.0		
146	91.0				
166	109.0				
181	121.0				
186	126.0				
191	135.0				

[a]Control points are based on comparisons of δ^{18}O data with V19-30, AMS dates, and correlation of planktonic foraminiferal abundances between cores.

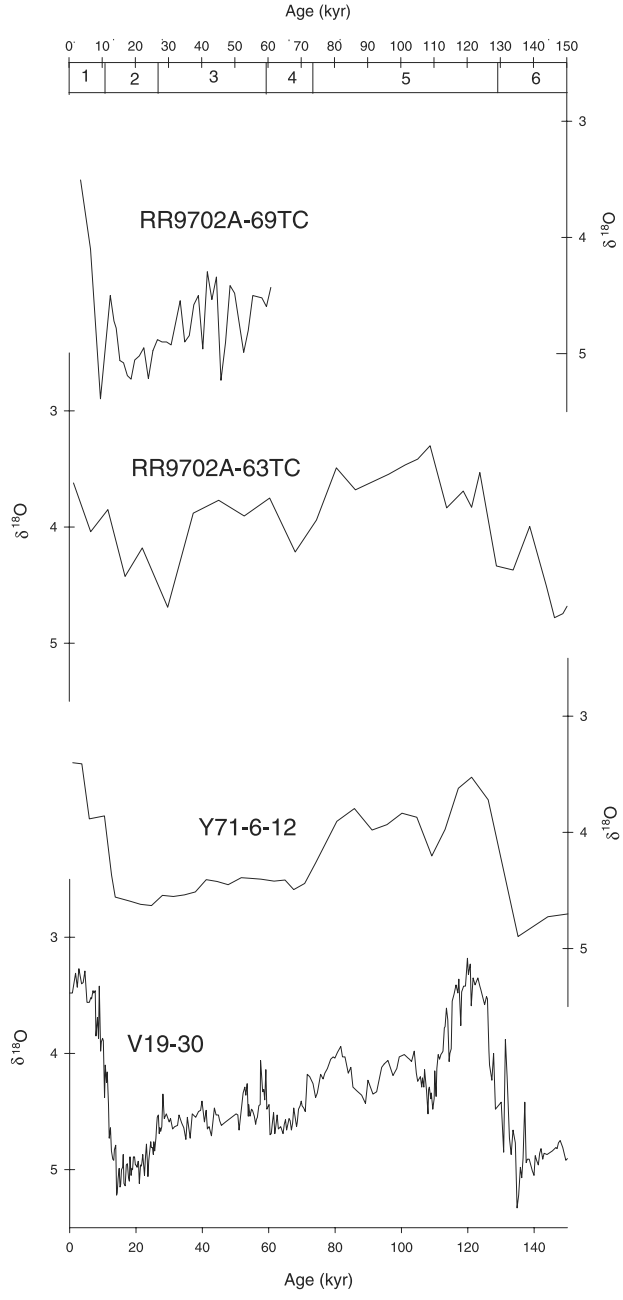

Figure 2. $\delta^{18}O$ versus age for (top to bottom) RR9702A-69TC, RR9702A-63TC, and Y71-6-12, V19-30, based on the benthic foraminifera *C. wuellerstorfi* and *U. perigrina*. The $\delta^{18}O$ data from *C. wuellerstorfi* were increased by 0.64 per mil and averaged with *U. perigrina* data at the same depths to create a single $\delta^{18}O$ record. Marine isotope stage boundaries are given on the upper x axis.

using the program CABFAC [*Klovan and Imbrie*, 1971]. A log transformation of the species percentages makes the species distribution Gaussian (which is appropriate for a factor model), and increases the importance of less abundant species [*Mix and Morey*, 1996; *Mix et al.*, 1999].

[22] Q-mode factor analysis of the foraminiferal species abundances in 767 core-top and down-core samples reveal four statistically independent assemblages, the "Equatorial," "Subpolar," "Subtropical," and "Eastern Boundary Current (EBC)" factors, which explain 90% of the total data [*Feldberg and Mix*, 2002]. These factors are named for their primary geographical distributions in the modern ocean. Loadings of the four factors in 69TC, 63TC, and Y71-6-12 exhibit significant variations over the last 150,000 years, and provide insight into the mechanisms of variability in the Peru Current through time (Figure 4).

[23] The "Subtropical" factor, comprised primarily of *G. ruber*, *G. sacculifer* and *G. glutinata*, is associated with warm oligotrophic water in the southern subtropical gyre [*Feldberg and Mix*, 2002]. Loadings of this factor are generally low (0.0–0.2) in 63TC and Y71-6-12 from 150 ka to 100 ka. At ~75 ka loadings drop below zero in both cores and then increase gradually to the present. In all three of the Nazca Ridge cores, the "Subtropical" factor is most prevalent within the Holocene (last 10,000 years). The range of variation of this factor is higher in the cores 63TC and Y71-6-12, which are closer to the center of the subtropical gyre, than in core 69TC, which is closer to the continental margin and coastal upwelling system.

[24] The "Equatorial" factor, comprised primarily of *N. dutertrei* and *P. obliquiloculata*, is associated with the productive equatorial upwelling system in the eastern Pacific [*Feldberg and Mix*, 2002]. Loadings of this factor in 63TC and Y71-6-12 decrease from 150 ka to the MIS 5/6 boundary (~128 ka), but then increase to relatively high values within last interglacial interval. Loadings decrease within MIS 2–4, although the details of the changes in this interval vary between cores. In core 63TC, the transition to lower values appears to occur earlier (~75 ka) than in core Y71-6-12 (~65 ka). This could in part reflect uncertainties in correlations between cores, but it also could reflect true diachroneity. In this interval, we did not adjust the timescale to force a faunal correlation, because it would have resulted in a distinct mismatch in the oxygen isotope records. The Equatorial factor returns to high values during the Holocene in all the cores. The greatest range in loadings of this factor is observed in core 69TC, perhaps because of its higher sedimentation rate (and thus lower impact of bioturbation) or because of a true difference in the fauna here based on its position close to the coast of South America near the edge of the gyre. As a result, the variations in the equatorial and subpolar faunas are larger, and the variations in the subtropical fauna are more subdued, in core 69TC than at the other sites.

[25] The "EBC" factor is defined by highly positive factor scores for the species *N. pachyderma* (dextral), *N. dutertrei*, and *P. obliquiloculata*, and negative scores for *G. bulloides*. In core-top sediments, this factor has its highest loadings along the west coast of South America, but relatively low values in the northern Peru Current [*Feldberg and Mix*, 2002]. The "EBC" factor is most prevalent in 63TC from ~70–85 ka, and in Y71-6-12 from ~60–80 ka. After 60 ka, loadings decrease to modern values in 63TC and Y71-6-12 but are intermittently elevated in 69TC.

[26] The "Subpolar" factor, highest in the species *G. bulloides*, *N. pachyderma (dextral)*, *N. pachyderma (sinis-*

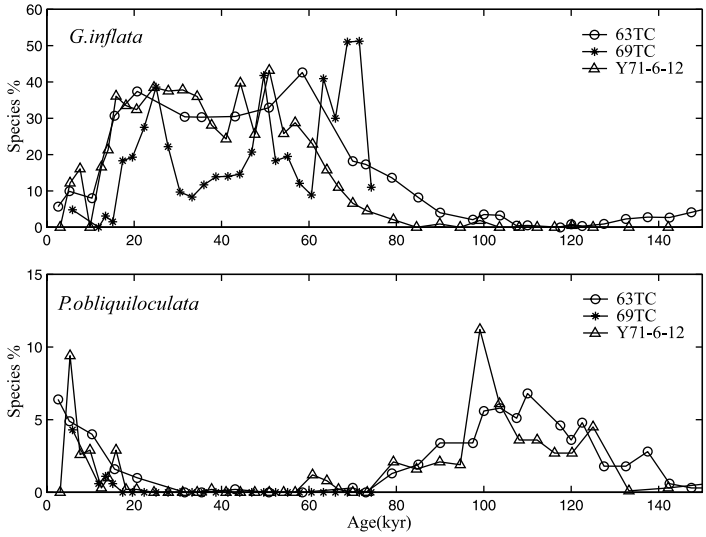

Figure 3. Percentages of *G. inflata* and *P. obliquiloculata* in Y71-6-12, RR9702A-69TC and RR9702A-63TC versus age. The timing of species abundance changes was used to help constrain the correlations between these cores.

tral), and *G. inflata*, is associated with cold waters off Southern Chile in modern core-top samples [*Hebbeln et al.*, 2000; *Feldberg and Mix*, 2002]. The dominant species in this factor are often associated with subsurface habitats, and thus we expect that incursions of these species into low latitudes may reflect changes in both surface and subsurface watermasses. This factor is less important in modern sediments off the coast Peru, but abundant here during the LGM and older intervals. Loadings are high (>0.8) at 150 ka and begin to decrease prior to the start of MIS 5. Near 60 ka the Subpolar factor loadings in 63TC and Y71-6-12 increase and remain high with some fluctuations through the LGM. Loadings of this factor are high (>0.7) but variable near the beginning of the 75 k.y. record of 69TC. At ~20 ka the factor loadings begin to decrease in all of these cores, reaching minimum values in the most recent samples. Changes in the abundance of the "Subpolar" factor are roughly coincident with, but in the opposite sense of, variations in the "Equatorial" factor at these sites. As with the "Equatorial" factor (and unlike the "Subtropical" factor) the largest changes in the "Subpolar" factor are observed in 69TC, the core closest to the coast, and the smallest changes are in core 63TC, the core farthest from the coast.

5.2. Paleotemperature Estimates

[27] The sediment records from Nazca Ridge provide both temporal and spatial information regarding changes in SST in the Peru Current over the last full glacial cycle (Figure 5). The total range of temperature changes here appears to be quite high, >12°C at Site 69TC, about 10°C in core Y71-6-12, and about 8°C in core 63TC. The general pattern of SST change at these sites is similar over the last 150,000 years. A similar pattern is also found based on the U^k_{37} proxy in core TG7 [*Calvo et al.*, 2001], located near core 63TC, although the total range of temperatures based on U^k_{37} (about 5°C) is lower than changes based on the foraminifera.

[28] Temperatures at Y71-6-12 and 63TC are 12–15°C from 150 ka to the beginning of MIS 5. At 130 ka warming begins and temperatures in both cores increase to ~20°C in stage 5e, comparable with modern temperatures in the region. Warmest SSTs appear to be slightly younger than MIS 5e, however, spanning the interval ~110–120 kyr in core Y71-6-12. In core 63TC, there are three warm peaks in SST during MIS 5 (90 ka, 104–108 ka, and 117 ka), while core Y71-6-12 has only two SST maxima (95 ka and 109 ka).

[29] Significant cooling occurs off Peru between 95 and 80 ka. After 80 ka the SST records diverge as 63TC continues to cool to 12°C and Y71-6-12 warms to 16°C. Temperatures in Y71-6-12 remain near 16°C until ~45 ka, after which they decrease to approximately 12°C. Younger than this time, the cores again have similar temperature records.

[30] In the interval from ~80 to ~50 ka, SST estimates in core Y71-6-12 are 2–3°C warmer than those of core 63TC. This is surprising, as 63TC is approximately 270 km farther offshore and is located in more subtropical waters than Y71-6-12. The temperature difference appears to be driven by a substantially higher "Equatorial" and slightly lower "Subpolar" factor loadings in Y71-6-12 than in 63TC during that time interval. This does not appear to be an artifact of timescale errors, and may reflect transport of the equatorial fauna southward in the Peru-Chile Countercurrent to the site of Y71-6-12 along with an offshore shift of the northward flowing Peru Current.

[31] Our SST estimates for 69TC begin at 75 ka and display a similar pattern to those of the other two cores. SSTs are typically cooler at 69TC than at the other two sites, consistent with its position closer to the continent, and near the coastal upwelling system. Short-term variations in SST within MIS 2–4, which are probably not completely resolved by our sampling, are quite large, and

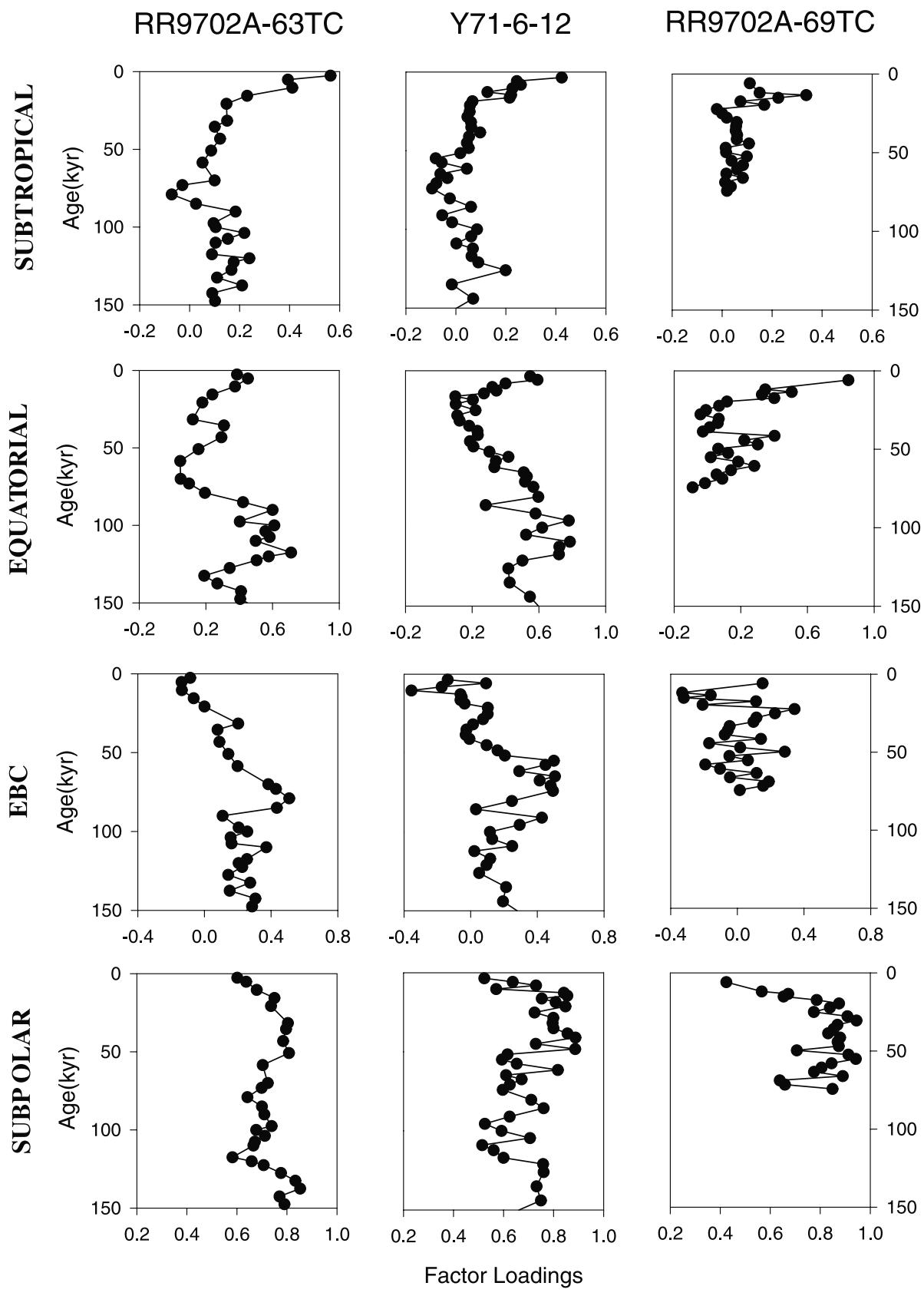

Figure 4. Faunal factors for RR9702A-63TC, Y71-6-12, and RR9702A-69TC plotted versus age. Factors from top to bottom are "Subtropical," "Equatorial," "EBC," and "Subpolar," with names based on their distribution in the modern ocean [*Feldberg and Mix*, 2002].

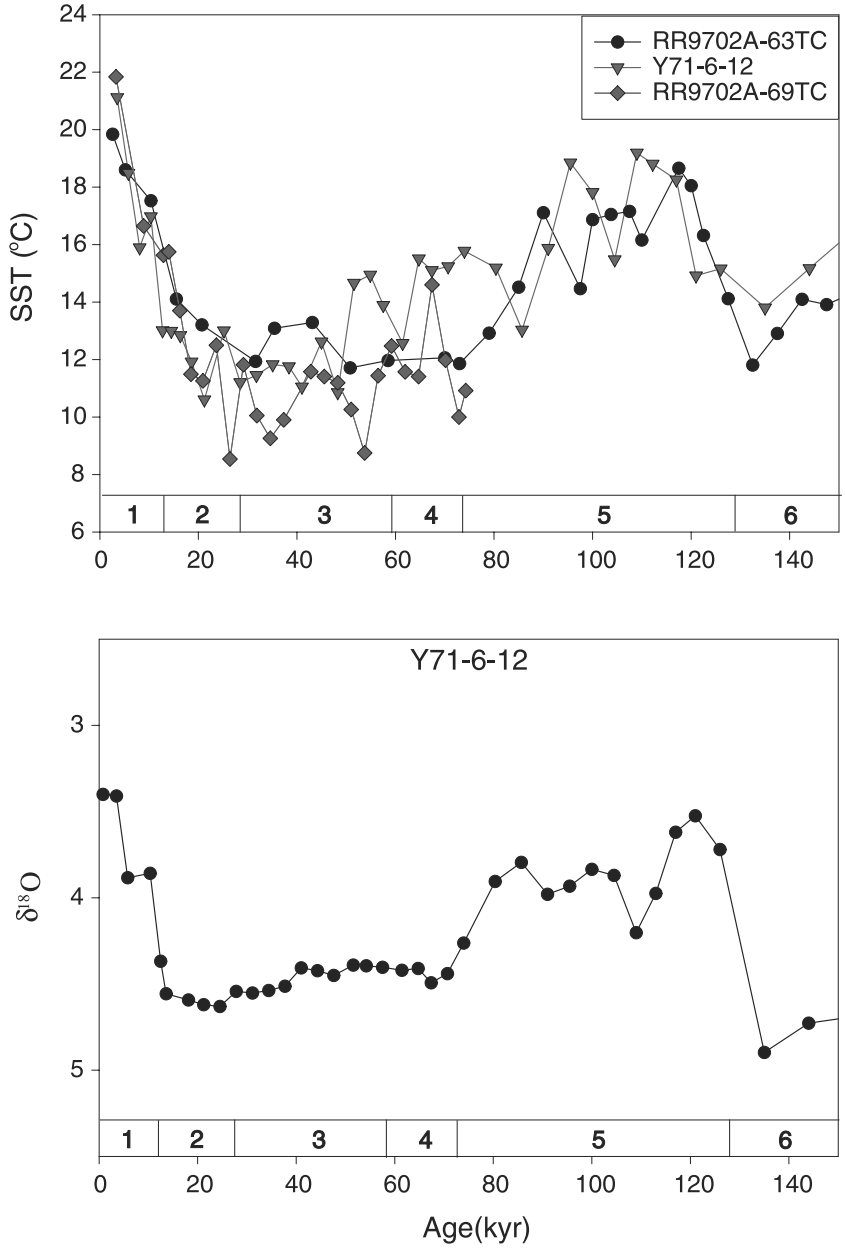

Figure 5. SST estimates versus age for Y71-6-12, RR9702A-63TC, and RR9702A-69TC. The $\delta^{18}O$ data from Y71-6-12 is given in the lower graph for reference. MIS stage boundaries are given at the bottom of both graphs.

range up to 6°C suggesting the likelihood that more detailed studies will detect millennial-scale climate changes in this region.

6. Discussion

6.1. Variations in the Peru Current

[32] Based on a shift of the cool water "Subpolar" faunal factor northward along the eastern boundary during the LGM, *Feldberg and Mix* [2002] concluded that LGM cooling off Peru and in the Eastern equatorial Pacific was largely a result of an increase in the strength of the Peru Current relative to today. This finding is consistent with cooling of the Peru Current off central Chile [*Marchant et al.*, 1999], sedimentological evidence for an equatorward shift and strengthening of southern westerly winds [*Lamy et al.*, 1999], along with the presence of subpolar species in multiple faunal groups along the equator [*Pisias and Mix*, 1997; *Mix et al.*, 1999], as well as with isotopic evidence for limited change in pycnocline depth associated with the LGM at the equator [*Faul et al.*, 2000]. Using the downcore records from 69TC, Y71-6-12, and 63TC, we can evaluate whether SST changes in this region are consistently associated with variations in the abundance of "Subpolar" fauna, and therefore changes in the strength of the Peru Current.

Table 3. Correlation Coefficients of Faunal Factors and SST for 69TC, Y71-6-12, and 63TC

	RR9702A-69TC	Y71-6-12	RR9702A-63TC
Equatorial	0.90	0.87	0.83
Subpolar	−0.87	−0.88	−0.75
Subtropical	0.61	0.18	0.57
EBC	−0.23	0.10	−0.36

[33] At the Nazca Ridge sites, the ''Equatorial'' and ''Subpolar'' factors are highly correlated with changes in SST over the last 150,000 years (Table 3). The ''Equatorial'' factor typically dominates the region during warmer (roughly interglacial) periods and is replaced by the ''Subpolar'' fauna during cooler (roughly glacial) intervals. We suggest that during the cooler intervals the strength of the Peru Current increased, extending the range of subpolar species northward together with cool water advection along the eastern boundary, while confining the range of the equatorial species to lower latitudes. In the warmer intervals the current strength decreased, SSTs warmed, and fauna associated with equatorial upwelling again inhabited the waters off the coast of Peru.

[34] In some cases, during transitions from cooler to warmer SSTs, such as during the MIS 5/6 deglaciation, the ''Equatorial'' fauna appears to have expanded at the expense of the ''Subpolar'' fauna in the Peru Current. At the MIS 2/1 boundary, however, the ''Subpolar'' and ''EBC'' factors were replaced by a combination of the ''Equatorial'' and ''Subtropical'' factors, resulting in even greater estimated changes in SST than at earlier transitions. Cooling during the MIS 2 and 6 glacial intervals was associated primarily with an increase in the ''Subpolar'' factor, while cooling during MIS 4 is related to an increase in the ''EBC'' fauna. These differences in the overall relationship of faunal factors to SST at various times indicate there are additional processes associated with some climatically important events to those that appear to dominate the overall record off Peru.

6.2. Deconvolving Influences of Advection and Upwelling on the Eastern Equatorial Pacific

[35] SSTs in the eastern equatorial Pacific have varied by >5°C over the last 150,000 years as seen in radiolarian [*Pisias and Mix*, 1997] and foraminiferal [*Mix et al.*, 1999] temperature estimates from core RC13-110, as well as in Mg/Ca temperature estimates from a nearby core [*Lea et al.*, 2000]. Our inference that changes in the strength of the Peru Current play a crucial role in determining SSTs along the eastern boundary of South America may help to elucidate the mechanisms of temperature change in the eastern equatorial Pacific.

[36] At present, two primary mechanisms contribute to the temperature of the equatorial cool tongue: variations in advection of cool water off the eastern boundary and changes in the rate of equatorial upwelling [*Wyrtki*, 1981; *Bryden and Brady*, 1985]. Here we use the simple heat budget model of *Feldberg and Mix* [2002], which considers these two dominant effects on the equatorial ocean, coupled to time-varying input based on our estimates of SST in the Peru Current to predict the effect of changes in Peru Current advection on SST at equatorial core RC13-110 through time. By examining the differences between this model prediction and the observed patterns of change along the equator, we can estimate the effects of local upwelling. To create an integrated SST record of the Peru Current for input into our heat budget model, we averaged the foraminiferal SST estimates for Y71-6-12 and 63TC in the time domain.

[37] *Feldberg and Mix* [2002] simplified the *Bryden and Brady* [1985] model by combining the input and output terms to give net vertical and horizontal temperatures and fluxes (Figure 6). The temperature of the equatorial waters (T_{eq}) in this model is given by:

$$T_{eq} = \frac{\left(f_{up}{*}T_{up}{*}\rho C_p\right) + \left(f_{ad}{*}T_{ad}{*}\rho C_p\right) + Q_n}{\left(f_{up}{*}\rho C_p\right) + \left(f_{ad}{*}\rho C_p\right)}$$

where f_{up} is the upwelling flux, T_{up} is the temperature of the upwelled water, f_{ad} is the advective flux, T_{ad} is the temperature of the advected water, Q_n is the radiative heat flux (net solar heating), ρ is the density of seawater and C_p is the heat capacity. Our model employs modern transport and temperature values of 15 Sv, 24°C for the Peru Current, and 27 Sv, 22°C for equatorial upwelling, respectively. Q_n is set at 5.7×10^{14} W. With these boundary conditions, the model produces a modern SST of 26°C for equatorial surface water, somewhat warmer than present values at the site of RC13-110, but broadly similar to values averaged along the equator in the Pacific Ocean.

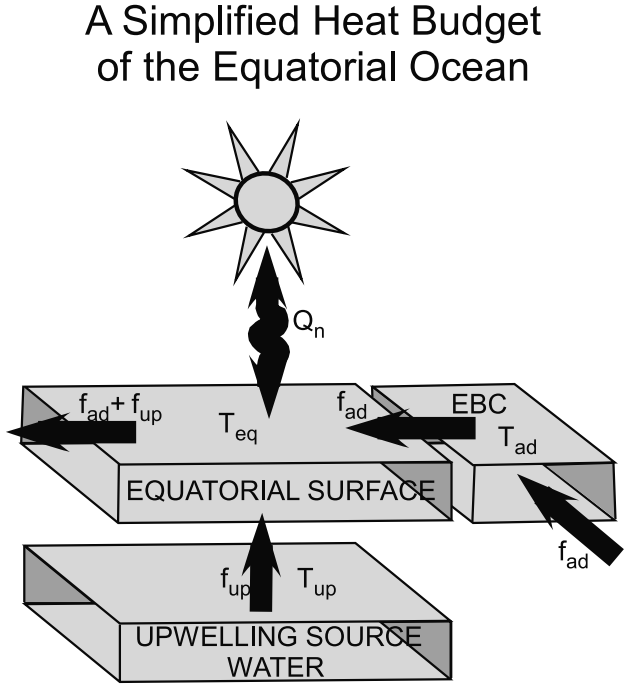

Figure 6. Cartoon illustrating the inputs and outputs used in the heat budget model, where f_{up} is the upwelling flux, T_{up} is the temperature of the upwelled water, f_{ad} is the advective flux from the Peru Current, T_{ad} is the temperature of the water advected off the eastern boundary, and Q_n is the net radiative heat flux.

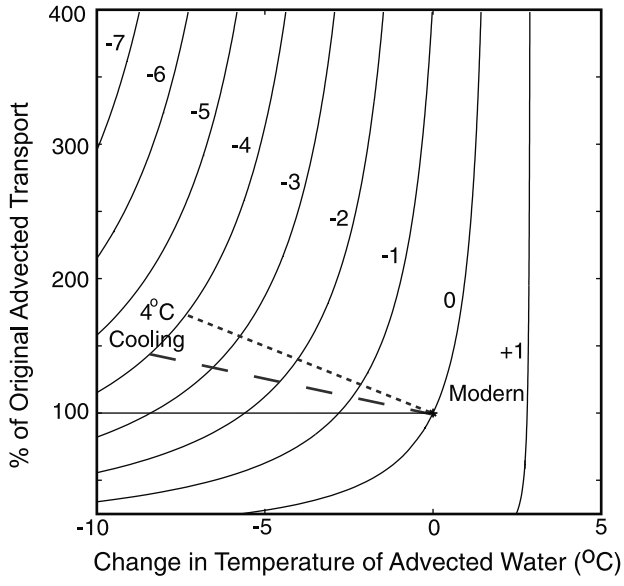

Figure 7. Heat budget model results showing changes in the temperature of equatorial Pacific surface waters relative to modern conditions (contours) resulting from changes in the temperature and advective transport of water in the Peru Current (Here straight lines demarcate a field of plausible changes in Peru Current advection and temperature that could account for 4°C cooling of equatorial waters).

[38] For purposes of sensitivity tests, we hold Q_n constant, because on an annual average basis radiation at the top of the atmosphere changed relatively little over the past 150,000 years [*Laskar et al.*, 1993] (although seasonal changes may have been significant). One might imagine a case in which Q_n varies substantially, for example due to increased cloud cover or atmospheric dust that reflects sunlight and shades the ocean. Such effects would have to be unreasonably large to account for the observed changes in SST. For example, a 3°C change in SST would require a 90% decrease in Q_n (assuming no other changes in boundary conditions). Within the modern tropics, mean annual radiative heat flux to the ocean varies only on the order of 10% [*Peixoto and Oort*, 1992], in part because high clouds associated with tropical convection have relatively small net effects on the radiation budget [*Ramanathan et al.*, 1989]. The effect of low stratus clouds is likely to be stronger, but preliminary evidence suggests that such clouds tend to act as a local negative feedback on temperature changes at the surface [*Miller*, 1997]. This tells us that variations in the annual-average radiation budget, although probably linked in some way to climate, are unlikely to be the primary cause of equatorial SST changes we have observed.

[39] While admitting the simplicity of our model, we will employ it to explore possible causes of tropical SST variations associated with upwelling and advection. First, we examine a range of sensitivity tests to assess the effects of advection off the eastern boundary on equatorial SST. The contours in Figure 7 indicate that when the temperature of advected water is relatively high or advective rates are high, equatorial temperatures are relatively insensitive to changes in advective transport but are responsive to temperature changes in the Peru Current. When advective transport is low and the temperature of the Peru Current is low, changes in transport have a greater influence on equatorial waters than small changes in the temperature of the Peru Current.

[40] Using our observations of changing SST in the Peru Current as a measure of watermass properties of the eastern boundary influence in the model, we can calculate the effect of a changing Peru Current on equatorial SSTs. We consider three scenarios for relative changes in equatorial SST in response to changes along the eastern boundary. In the first model case (solid horizontal line in Figure 7), we assume no change in the rate of advection from the eastern boundary, but adjust the temperature of the advected Peru Current water. In this case, Peru Current cooling of >10°C is needed to account for the observed ~4°C cooling of the equatorial cold tongue. This case is plausible only if the extreme cooling we observed (at core 69TC) is representative of the Peru Current as a whole (which we consider unlikely). It begs the question of what caused the Peru Current cooling, if no increase in advection occurred. In the second case (dashed line in Figure 7), we assume that advection increased by 50% for each 10°C decrease in Peru Current SST. This case yields a 4°C equatorial cooling from an 8°C cooling of the Peru Current (within the range of our estimates) and a modest (50%) increase in advection from 15 to 22 Sv. In a third case (dotted line in Figure 7), each 10°C decrease in eastern boundary current temperature is assumed to correspond to a doubling of advection. This case requires less cooling of the Peru Current (~7°C) and a slightly greater increase in advection (~80%) to account for a 4°C cooling at the equator. We consider these two scenarios of Peru Current cooling associated with some increase in advection as plausible causes of LGM cooling at the equator [*Feldberg and Mix*, 2002].

[41] We project the results of the advection model through time using the time history of SST off southern Peru to predict the temporal effects of temperature changes here on the equatorial cool tongue (Figure 8). We then compare these model results to estimates of SST change in core RC13-110, which we take as representative of the equatorial cold tongue. In Figure 8, we also compare our SST estimates based on planktonic foraminiferal assemblages in core RC13-110 to independent SST estimates based on Mg/Ca in nearby core TR163-19 [*Lea et al.*, 2000]. Although the SSTs in TR163-19 are, on average, about 2°C warmer than those in RC13-110, such an offset is consistent with the differences in modern SSTs between the two locations. Glacial-interglacial variations in SST at the two sites based on two different methods are remarkably similar in both timing and amplitude of changes. Slight offsets in the amplitude of change between the two sites occurs within the interval of MIS 5 (especially from ~75–105 ka), but overall the fit is good and use of one curve or the other in our analysis would not substantially change our conclusions. Both the foraminiferal species record from RC13-110 and the Mg/Ca SST estimates from TR163-19 appear discordant with recent estimates of SST based on a shorter

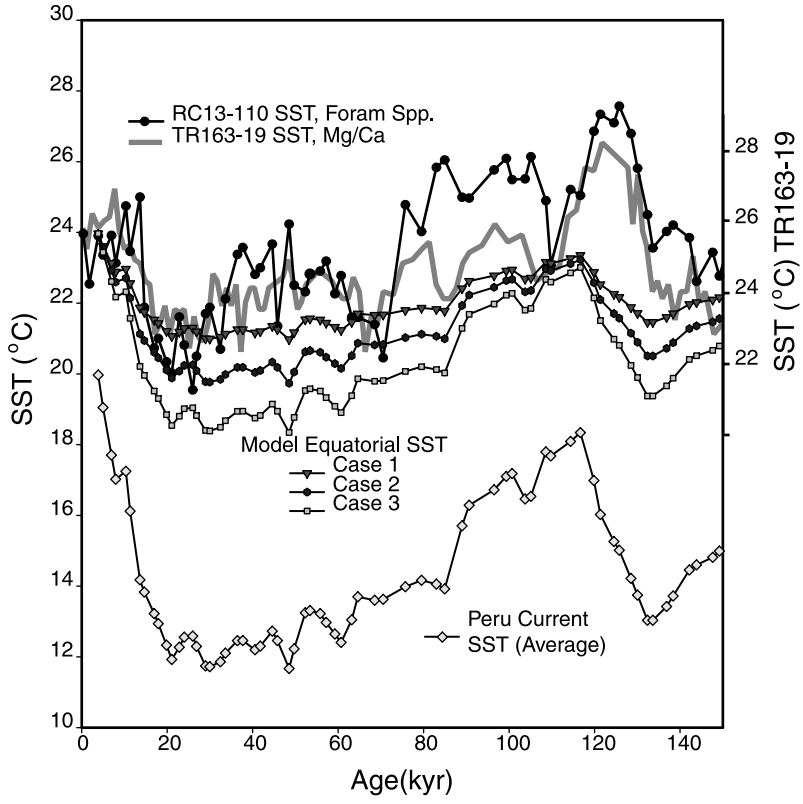

Figure 8. Foraminiferal SST estimates from the Peru Current (diamonds, average of Y71-6-12 and RR9702A-63TC) and three predictions of changes in equatorial SST associated with changing advection off the eastern boundary, assuming (1) Peru Current cooling with no change in advective transport (triangles), (2) a 50% increase in advection rate for each 10°C cooling of the Peru Current (hexagons), and (3) a doubling of advection for each 10°C cooling of the Peru Current (squares). SST estimates at equatorial site RC13-110 (circles) indicate that most of the observed changes associated with the LGM (~21 ka BP) can be attributed to changes in the Peru Current, but other changes in equatorial temperature can not. For comparison the Mg/Ca temperature estimates at site TR163-19 [*Lea et al.*, 2000] are shown (gray line, scale at right).

time series of Mg/Ca in a shallow water core from the Galapagos Platform. These estimates suggest late Holocene SST values of about 22°C, somewhat colder than modern mean annual SST values at the site (24°C), and with relatively little change in temperature between modern and LGM conditions [*Koutavas et al.*, 2002]. The cause of the apparent disagreement between the Mg/Ca SST estimates at the two sites remains unclear, but we question whether local island-effect upwelling at the shallow water site coupled to subsurface habitats and seasonal species blooms may contribute to the anomalous results of *Koutavas et al.* [2002]. We continue to use the foraminiferal results from RC13-110 as representative of general trends of SST change within the equatorial cold tongue where it is well developed west of Galapagos.

[42] Model results for the first case, in which advection was held constant at modern values, indicate that a decrease in temperature of the Peru Current alone can produce significant changes at the equator but not enough to account for the observed SST variations at RC13-110 (Figure 8). Increasing the rate of advection in the current proportional to cooling of the Peru Current serves to increase the amplitude of change and to decrease the mean temperature near the equator. In the second test case, equatorial SSTs of the LGM can be explained entirely by changes in the eastern boundary current, and in the third case, predicted equatorial SSTs are even colder than those observed. Using an ocean modeling experiment, *Andreasen et al.* [2001] noted a substantial increase in advection into the equatorial cold tongue, consistent with our inferences, but did not specifically link SST variability at the equator to this advection.

[43] In spite of success of the model in simulating LGM temperature change at the equator based on our estimated temperatures off Peru [*Feldberg and Mix*, 2002], plausible changes in the Peru Current cannot account for all of the equatorial SST variations recorded at RC13-110 over the last 150,000 years (Figure 8). Our model results suggest that about half of the total variance in equatorial Pacific temperatures is related to changes in the Peru Current. Distinct differences between the time series of equatorial SST predicted by our model in response to changes in the Peru Current and the SST changes we estimated from foraminiferal faunas at RC13-110 indicate that another process, such as local upwelling, must be important in controlling equa-

torial SSTs. We next explore possible causes of these additional changes at the equator.

[44] To partition equatorial SST changes into components related to advection and upwelling, we calculate the difference between the SSTs we estimated at RC13-110 (Figure 8) and the time series of equatorial SSTs predicted by our model test case 2 for a changing advective component alone. These temperature residuals, which range from −1 to +5°C (Figure 9a), are the portion of the paleotemperature record at RC13-110 that cannot be explained by advection of cool water from the Peru Current. Within the constraints of our heat budget model, we interpret this component of SST to be the result of variations in local equatorial upwelling or pycnocline depth. For comparison, equatorial SST anomalies related to the eastern boundary component vary by about 4°C. Although the LGM exhibited little difference in the equatorial upwelling component of SST relative to modern conditions (consistent with *Faul et al.* [2000]), clearly at other times the variations in equatorial upwelling were as large or larger than variations in the eastern boundary current.

[45] Temperature anomalies associated with changing equatorial upwelling (Figure 9a) are mostly positive, because the SSTs estimated at RC13-110 are often warmer than those predicted by the model based on input from the Peru Current. Positive SST residuals here imply that upwelling was weaker (or that the upwelling source water was warmer) than at present. Conversely, negative SST anomalies imply that upwelling was stronger (or source waters were colder). In other words, although the modern (late Holocene) Peru Current influence is relatively weak along the equator (compared to its glacial mode), the modern upwelling within the equatorial cold tongue is in its strong (cold) mode.

[46] As for the case of Peru Current advection, we can use our simple heat budget model to explore quantitatively how changes in upwelling could be translated into changes in equatorial SST. In Figure 10, contours denote changes in SST in response to changes in upwelling rate (percentage of modern values, vertical axis) and changes in the temperature of upwelling source waters (which could also be interpreted as related to pycnocline depth, horizontal axis). Within the framework of this simple model, a plausible scenario to account for a 5°C warming in the upwelling component of SST (as observed in Figure 9a) is a reduction in the rate of upwelling to 25% of the modern values coupled to a 5°C increase in the temperature of upwelling waters. This implies a deeper thermocline (solid line in Figure 10) or a slightly greater reduction in upwelling with no change in source water temperature (dotted line in Figure 10). To account for a negative (cool) SST residual of 1°C in Figure 9a would require either a 50% increase in equatorial upwelling with no changes in source water temperature, or a smaller increase in upwelling rate with a 1°C cooling of source waters. Both of these scenarios imply significant changes in the rate of upwelling along the equator, which presumably relate to forcing by equatorial winds.

6.3. Possible Causes of SST, Advection, and Upwelling Changes

[47] Our estimate of the temporal variations in the eastern-boundary advection contribution to equatorial SST change appears broadly similar to the record of high-latitude climate changes recorded by benthic foraminiferal $\delta^{18}O$ (reflecting changes in global ice volume and deepwater temperature, both of which respond to high-latitude climates). This relationship suggests that changes in the strength and/or temperature of the Peru Current at low latitudes occurred in response to the growth and retreat of the polar ice sheets or aspects of the global climate system that roughly covary with high-latitude climate. This primary conclusion is independent of the details of timescales.

[48] To compare with other data sets, we allow for some uncertainty in the SPECMAP timescale, and in Figure 9 plot the our inferred upwelling and advective components of equatorial temperature on the original SPECMAP timescale (light gray lines without symbols) and with an age model stretched by 5% (solid line with symbols), which allows for an MIS 5/6 boundary at 135 ka based on U-Th dates [*Henderson and Slowey*, 2000]. With the modified timescale, the eastern-boundary component of SST change (Figure 9b) mimics variations in atmospheric CO_2 variations recorded in the Vostok ice core [*Petit et al.*, 1999]. This relationship makes sense if glacial cooling at high latitudes increased hemispheric thermal gradients and thereby strengthened wind-driven gyre circulation [*Rind*, 1998]. In this regard we agree with the findings of *Lea et al.* [2000], who hypothesized a link between polar and tropical temperature changes in the Southern Hemisphere based on some similarity of Mg/Ca variations near the equator with isotopic changes in Antarctic ice cores. However, we extend and modify this hypothesis by partitioning the equatorial SST responses into their high-latitude (advective) and low-latitude (upwelling) components.

[49] The contribution of equatorial upwelling to SST variations in the eastern equatorial Pacific (Figure 9a) exhibits a temporal pattern similar to a model prediction of temperature variations based on orbitally forced variations in El Nino frequency [*Clement and Cane*, 1999], assuming the stretched age model is correct. *Beaufort et al.* [2001] inferred changes in biological productivity associated with east-west pycnocline slope in the Pacific based on calcareous nannofossil and also suggested a link to interannual El Niño-Southern Oscillations (ENSO) events using a similarly stretched time scale. A link of high production along the equator (as reflected in pycnocline-sensitive nannofossil species of *Beaufort et al.* [2001]) to cold temperatures is plausible. The paleo-ENSO model of *Clement and Cane* [1999] predicts changes in ocean temperature (averaged over the Niño-3 region) of less than 1°C, whereas our estimate of SST variations associated with changing upwelling span a range of about 5–6°C (Figure 9a), a clear mismatch in amplitude. The paleo-ENSO model assumes modern boundary conditions (other than insolation change), so perhaps other mechanisms will be found that amplify the model response to relatively small variations in insolation.

[50] One possible mechanism that could amplify tropical responses to insolation is the Asian monsoon [*Clement et al.*, 1999], which is thought to respond strongly to regional summer heating [*Prell and Kutzbach*, 1992]. A coupled atmosphere-ocean model experiment noted the sensitivity

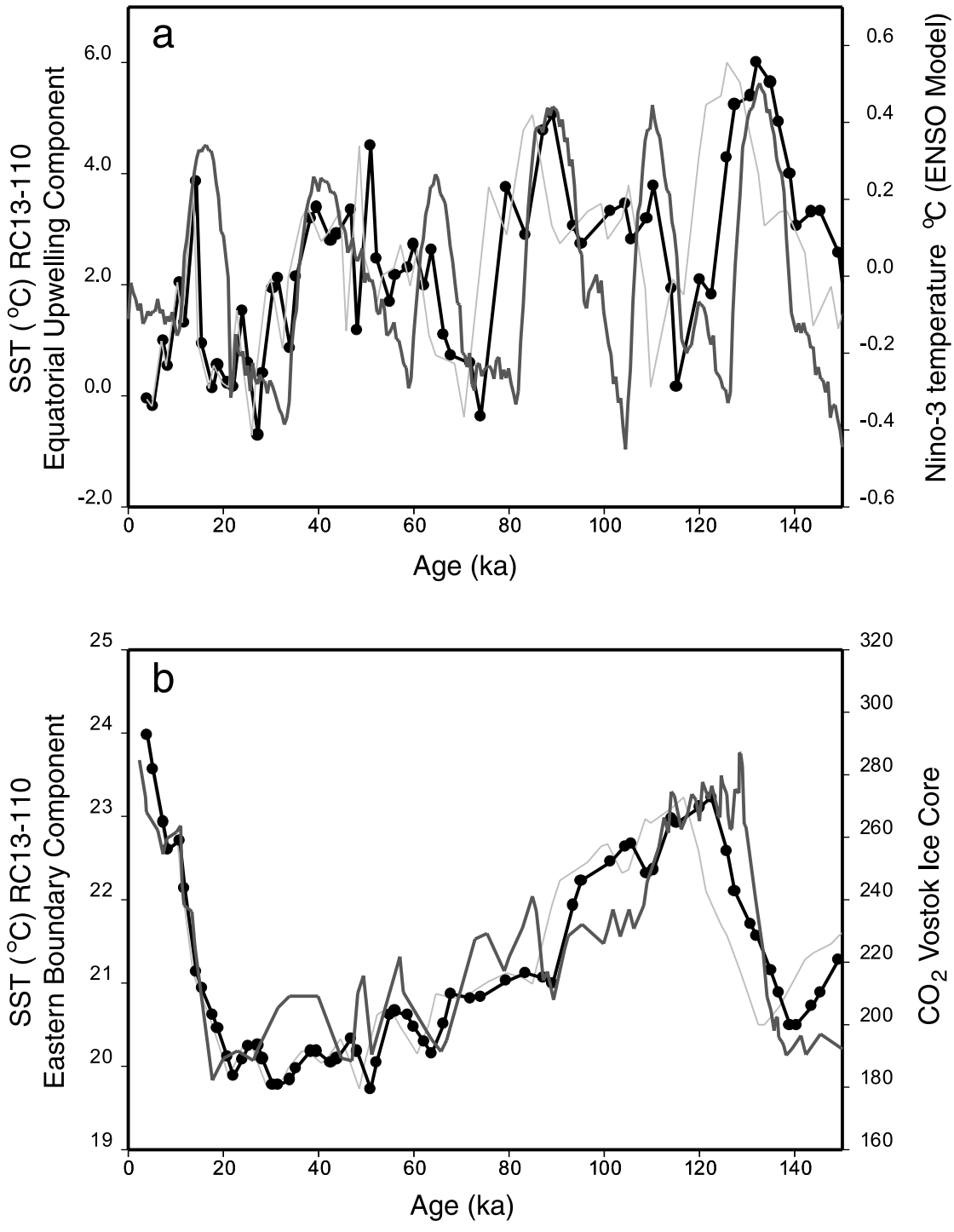

Figure 9. Components of equatorial SST changes at RC13-110 related to (a) equatorial upwelling, and (b) EBC advection, using case 2 from Figure 8. Time series here are based on the SPECMAP timescale (light gray line in Figures 9a and 9b), and on a stretched timescale that sets the MIS 5/6 boundary at 134 ka (black line with circles in a and b). For comparison, in panel a the dark gray curve is an estimate of changing annual SST associated with El Niño frequency (gray line) based on *Clement and Cane* [1999]. In Figure 9b, the dark gray curve is the atmospheric CO_2 as observed in the Vostok ice core [*Petit et al.*, 1999].

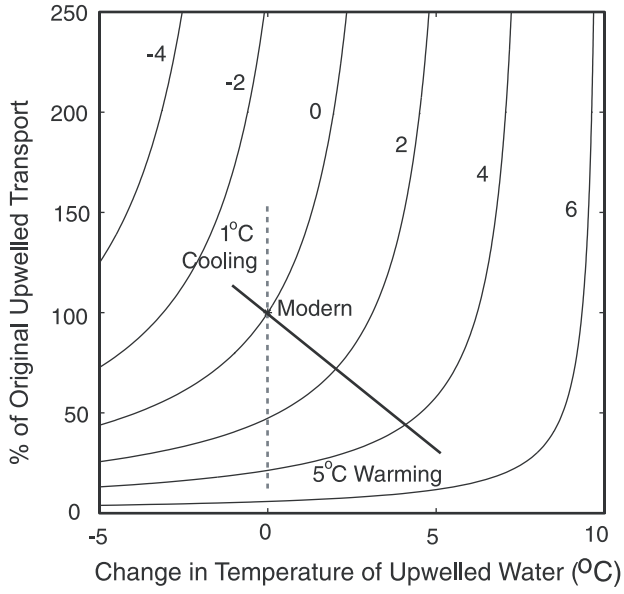

Figure 10. Heat budget model results showing changes in the temperature of equatorial Pacific surface waters relative to modern conditions (contours) that result from changes in the rate of equatorial upwelling (vertical axis) and temperature of upwelling source waters (horizontal axis). Straight lines demarcate a field of plausible changes in the upwelling system that could account for equatorial changes in sea surface temperature ranging from a 1°C cooling to a 5°C warming.

of equatorial upwelling and thermocline depth to remote (western Pacific) forcing during the last ice age [*Andreasen et al.*, 2001] but did not specifically address the potential for monsoonal or other insolation effects to modify the eastern equatorial Pacific. On an interannual scale, changes in eastern equatorial Pacific SST are sometimes associated with Asian monsoon intensity, but it remains controversial whether the ENSO state affects the monsoon [*Rasmussen and Carpenter*, 1983; *Ju and Slingo*, 1995] or the monsoon state modifies ENSO [*Yasunari*, 1990; *Webster and Yang*, 1992; *Wainer and Webster*, 1996]. Strong Asian monsoons in the western Indian Ocean are thought to lag Northern Hemisphere summer insolation changes, perhaps because they are retarded by snow and ice cover in Eurasia [*Clemens et al.*, 1991], and if so they would have phases inconsistent with changes in the upwelling component we infer in the eastern tropical Pacific. *Beaufort et al.* [1999] review evidence for upwelling and productivity signals in the central Indian Ocean, and suggest a more direct response of the equatorial winds to insolation in February (the equinox) for that region. These authors noted that variations in monsoon winds might have different phases in different regions. Given this complexity, although the link of monsoons to summer insolation may provide an attractive mechanism to amplify the response of upwelling in the eastern equatorial Pacific, the linkage remains speculative at present.

[51] Other data from the tropics suggest additional ways upwelling changes along the equator may be linked to the orbital cycles via variations in insolation. For example, *Lyle et al.* [1992] find coherency between orbital precession (23 k.y. period) and a SST record based on alkenones from the central equatorial Pacific. Seeking mechanisms to explain the observed changes in the equatorial system that lead changes in high-latitude ice volume, *Lyle et al.* [1992] speculated that high insolation in Southern Hemisphere winter reduced cross-equatorial gradients in solar heating and caused the intertropical convergence to migrate southward, yielding a relaxation of the equatorial winds and reduced upwelling. This hypothesis may be plausible for the precessional (23 k.y. period) component of insolation, but has the wrong phase for the obliquity (41 k.y. period) component of insolation.

[52] Whatever the ultimate mechanisms responsible for change, our observation that an equatorial component of temperature change preceded changes in $\delta^{18}O$ in the same samples indicates that such variations in equatorial upwelling did not respond simply to high latitude growth and retreat of the polar ice sheets. Similar early changes in climate have been observed elsewhere in the tropics [e.g., *Mix and Morey*, 1996; *Beaufort et al.*, 1999; *Schneider et al.*, 1999] and these widespread observations suggest either some climatic connection between areas, or the possibility that multiple mechanisms sensitive to insolation change can drive climate change within the tropics.

7. Summary and Conclusion

[53] Here we use a regional calibration equation based on planktonic foraminiferal faunas [*Feldberg and Mix*, 2002] to estimate Peru Current SST from three cores on the Nazca Ridge over the last 150,000 years. Temperature histories from the three sites reveal that temperatures off Peru have varied by as much as 10–12°C during the last glacial cycle.

[54] Changes in the abundance of the "Subpolar" and "Equatorial" faunas through time indicate that variations in the strength of the Peru Current are largely responsible for temperature changes along the eastern boundary of South America on glacial-interglacial timescales. During warm intervals, the Peru Current is weaker and fauna from the equatorial region inhabits the eastern boundary. During cooler times, when the strength of the current is increased, fauna from the subpolar regions is dominant in the Peru Current and the equatorial fauna is confined to the lower latitudes. "Subtropical" and "Eastern Boundary Current" fauna also vary significantly downcore.

[55] Using our temperature estimates in the eastern boundary current as input to a simple heat budget model, we predict the effect of advection on equatorial SSTs (core RC13-110), and estimate (as a residual) the contribution of changing equatorial upwelling or pycnocline depth to changes in equatorial SST through time. Allowing for timescale uncertainties, changes in the temperature of the eastern boundary current mimic changes in atmospheric CO_2 (as recorded in the Vostok ice core), suggesting a link to polar climate changes and hemisphere-scale wind systems.

[56] Equatorial upwelling west of Galapagos was not significantly stronger than at present during the LGM (21 ka) and the observed equatorial cooling at that time was mostly associated with changes in the strength and/or

temperature of advection off the eastern boundary. At other times, the variations in the equatorial upwelling component dominate over advection. The local upwelling component leads changes in polar climates as recorded in benthic foraminiferal $\delta^{18}O$, and varies essentially in phase with orbital forcing. Given allowances for timescale uncertainties, the patterns of variability in the equatorial component are remarkably similar to model prediction of variations in the frequency of El Niño events, although our estimated temperature changes are much larger than model predictions, suggesting the need for additional amplifying mechanisms. A clear implication is that the linkage between orbital changes and equatorial winds is both direct and rapid, and does not require changes in high-latitude ice sheets. A high-latitude influence enters the equatorial system later, via modification of the eastern boundary current.

[57] **Acknowledgments.** We thank Ann Morey and June Wilson for assistance with species identification, SST estimates, and ^{14}C sample preparation, Bill Rugh for mass spectrometry, and Sheila O'Keefe for assistance with heat budget calculations. We appreciate helpful reviews from Luc Beaufort and an anonymous reviewer that improved the paper. This work and core material curation at Oregon State University was funded by NSF.

References

Andreasen, D. H., A. C. Ravelo, and A. J. Broccoli, Remote forcing at the Last Glacial Maximum in the tropical Pacific Ocean, *J. Geophys. Res.*, *106*, 879–897, 2001.

Beaufort, L., F. Bassinot, and E. Vincent, Primary production response to orbitally induced variations of the southern oscillation in the equatorial Indian Ocean, in *Reconstructing Ocean History: A Window Into the Future*, edited by F. Abrantes and A. Mix, pp. 245–271, Kluwer Acad., New York, 1999.

Beaufort, L., T. de Garidel-Thoron, A. C. Mix, and N. G. Pisias, ENSO-like forcing on oceanic primary production during the late Pleistocene, *Science*, *293*, 2440–2444, 2001.

Broecker, W., A. Mix, M. Andree, and H. Oeschger, Radiocarbon measurements on coexisting benthic and planktic foraminifera shells: Potential for reconstructing ocean ventilation times over the past 20,000 years, *Nucl. Instrum. Methods Phys. Res., Sect. B*, *5*, 331–339, 1984.

Bryden, H. L., and E. C. Brady, Diagnostic model of the three-dimensional circulation in the upper equatorial Pacific Ocean, *J. Phys. Oceanogr.*, *15*, 1255–1273, 1985.

Calvo, E., C. Pelejero, J. C. Herguera, A. Palanques, and J. O. Grimalt, Insolation dependence of the southeastern subtropical Pacific sea surface temperature over the last 400 kyr, *Geophys. Res. Lett.*, *28*, 2481–2484, 2001.

Clemens, S. C., W. Prell, D. Murray, G. Shimmield, and W. Graham, Forcing mechanisms of the Indian Ocean monsoon, *Nature*, *353*, 720–725, 1991.

Clement, A. C., and M. A. Cane, A role for the tropical Pacific coupled ocean-atmosphere system on Milankovitch and Millennial timescales, I, A modeling study of tropical Pacific variability, in *Mechanisms of Global Climate Change at Millennial Time Scales*, *Geophys. Monogr. Ser.*, vol. 112, edited by P. U. Clark, R. S. Webb, and L. D. Keigwin, pp. 363–372, AGU, Washington, D. C., 1999.

Clement, A. C., R. Seager, and M. A. Cane, Orbital controls on the El Niño/Southern Oscillation and the tropical climate, *Paleoceanography*, *14*, 441–456, 1999.

CLIMAP, Seasonal reconstructions of the Earth's surface at the last glacial maximum, *Geol. Soc. Am. Map Chart Ser.*, *MC-36*, Boulder, Colo., 1981.

Crowley, T. J., CLIMAP SSTs re-revisited, *Clim. Dyn.*, *16*(4), 241–255, 2000.

Faul, K., A. C. Ravelo, and M. L. Delaney, Changes in upwelling, productivity, and photic zone depth in the eastern equatorial Pacific Ocean over the last 50,000 years: A foraminiferal isotopic and abundance study, *J. Foraminiferal Res.*, *30*, 110–125, 2000.

Feldberg, M. J., and A. C. Mix, SST estimates in the southeast Pacific based on planktonic foraminiferal species: Modern calibration and Last Glacial Maximum, *Mar. Micropaleontol.*, *44,* 1–29, 2002.

Hebbeln, D., M. Marchant, T. Freundenthal, and G. Wefer, Surface sediment distribution along the Chilean continental slope related to upwelling and productivity, *Mar. Geol.*, *164*, 119–137, 2000.

Henderson, G. M., and N. C. Slowey, Evidence from U-Th dating against Northern Hemisphere forcing of the penultimate deglaciation, *Nature*, *404*, 61–66, 2000.

Huyer, A., M. Knoll, T. Paluszkiewicz, and R. L. Smith, The Peru Undercurrent: A study in variability, *Deep Sea Res.*, *38*, suppl. 1, S247–S271, 1991.

Imbrie, J., and N. G. Kipp, A new micropaleontological method for quantitative paleoclimatology: Application to a late Pleistocene Caribbean core, in *The Late Cenozoic Glacial Ages*, edited by K. K. Turekian, pp. 71–147, Yale Univ. Press, New York, 1971.

Imbrie, J., J. D. Hays, D. G. Martinson, A. McIntyre, A. C. Mix, J. J. Morley, N. G. Pisias, W. L. Prell, and N. J. Shackleton, The orbital theory of Pleistocene climate: Support from a revised chronology of the marine δ18O record, in *Milankovitch and Climate*, *Proceedings of the NATO Workshop*, edited by A. Berger et al., pp. 269–305, D. Reidel, Norwell, Mass., 1984.

Ju, J., and J. Slingo, The Asian summer monsoon and ENSO, *Q. J. R. Meteorol. Soc.*, *121*, 1133–1168, 1995.

Klovan, J. E., and J. Imbrie, An algorithm and FORTRAN IV program for large-scale Q-mode factor analysis and calculation of factor scores, *Math. Geol.*, *3*(1), 61–77, 1971.

Koutavas, A., J. Lynch-Stieglitz, T. M. Marchitto Jr., and J. P. Sachs, El-Niño-like pattern in ice age tropical Pacific sea surface temperature, *Science*, *297*, 226–230, 2002.

Lamy, F., D. Hebbeln, and G. Wefer, High-resolution marine record of climatic change in mid-latitude Chile during the last 28,000 years based on terrigenous sediment parameters, *Quat. Res.*, *51*, 83–93, 1999.

Laskar, J., F. Joutel, and F. Boudin, Orbital, precessional, and insolation quantities for the Earth from −20 Myr to +10 Myr, *Astron. Astrophys.*, *270*, 522–533, 1993.

Le, J., A. C. Mix, and N. J. Shackleton, Late Quaternary paleoceanography in the eastern equatorial Pacific Ocean from planktonic foraminifers: A high resolution record from Site 846, in *Proceedings of the Ocean Drilling Program, Scientific Results*, *138*, edited by N. G. Pisias et al., pp. 675–687, Ocean Drill. Prog., College Station, Tex., 1995.

Lea, D. W., D. K. Pak, and H. J. Spero, Climate impact of late quaternary equatorial Pacific sea surface temperature variations, *Science*, *289*, 1719–1724, 2000.

Lyle, M. W., F. G. Prahl, and M. A. Sparrow, Upwelling and productivity changes inferred from a temperature record in the central equatorial Pacific, *Nature*, *355*, 812–815, 1992.

Marchant, M., D. Hebbeln, and G. Wefer, High resolution planktic foraminiferal record of the last 13,300 years from the upwelling area off Chile, *Mar. Geol.*, *161*, 115–128, 1999.

Miller, R. L., Tropical thermostats and low cloud cover, *J. Clim.*, *10*, 409–440, 1997.

Mix, A. C., and A. E. Morey, Climate feedback and Pleistocene variation in the Atlantic south equatorial current, in *The South Atlantic: Present and Past Circulation*, edited by G. Wefer et al., pp. 503–525, Springer-Verlag, New York, 1996.

Mix, A. C., and W. F. Ruddiman, Structure and timing of the last deglaciation: Oxygen isotope evidence, *Quat. Sci. Rev.*, *4*, 59–108, 1985.

Mix, A. C., N. G. Pisias, R. Zahn, W. Rugh, C. Lopez, and K. Nelson, Carbon-13 in Pacific deep and intermediate waters, 0–370 ka: Implications for ocean circulation and Pleistocene CO_2, *Paleoceanography*, *6*, 205–226, 1991.

Mix, A. C., A. E. Morey, N. G. Pisias, and S. W. Hostetler, Foraminiferal faunal estimates of paleotemperature: Circumventing the no-analog problem yields cool ice age tropics, *Paleoceanography*, *14*, 350–359, 1999.

Ocean Climate Laboratory, *World Ocean Atlas 1998*, 16 pp., Natl. Oceanogr. Data Cent., Silver Spring, Md., 1999.

Parker, F., Planktonic foraminiferal species in Pacific sediments, *Micropaleontology*, *8*, 219–254, 1962.

Patrick, A., and R. C. Thunell, Tropical Pacific sea surface temperatures and upper water column thermal structure during the last glacial maximum, *Paleoceanography*, *12*, 649–657, 1997.

Peixoto, J. P., and A. H. Oort, *Physics of Climate*, 520 pp., Am. Inst. Phys., New York, 1992.

Petit, J. R., et al., Climate and atmospheric history of the past 420,000 years from the Vostok ice core, Antarctica, *Nature*, *399*, 429–436, 1999.

Pisias, N. G., and A. C. Mix, Spatial and temporal oceanographic variability of the eastern equatorial Pacific during the late Pleistocene: Evidence from radiolaria microfossils, *Paleoceanography*, *12*, 381–393, 1997.

Prell, W. G., and J. E. Kutzbach, Sensitivity of the Indian monsoon to forcing parameters and implications for its evolution, *Nature*, *360*, 647–652, 1992.

Ramanathan, V., R. D. Cess, E. F. Harrison, P. Minnis, B. R. Barkstrom, E. Ahmad, and D. Hartman, Cloud-radiative forcing and the climate: Results from the Earth Radiation Budget Experiment, *Science*, *243*, 57–63, 1989.

Rasmussen, E. M., and T. H. Carpenter, The relationship between eastern equatorial Pacific sea surface temperatures and rainfall over India and Sri Lanka, *Mon. Weather Rev.*, *111*, 517–528, 1983.

Rind, D., Latitudinal temperature gradients and climate change, *J. Geophys. Res.*, *103*, 5943–5971, 1998.

Schneider, R. R., P. J. Müller, and R. Acheson, Atlantic alkenone sea-surface temperature records, low versus mid latitudes and differences between hemispheres, in *Reconstructing Ocean History: A Window Into the Future*, edited by F. Abrantes and A. Mix, pp. 33–55, Kluwer Acad., New York, 1999.

Shackleton, N. J., The 100,000-year ice-age cycle identified and found to lag temperature, carbon dioxide, and orbital eccentricity, *Science*, *289*, 1897–1902, 2000.

Shackleton, N. J., and N. G. Pisias, Atmospheric carbon dioxide, orbital forcing, and climate, in *The Carbon Cycle and Atmospheric CO_2: Natural Variations Archean to Present*, edited by E. T. Sundquist and W. S. Broecker, pp. 303–317, AGU, Washington, D. C., 1985.

Strub, T. P., J. M. Mesías, and C. James, Altimeter observations of the Peru-Chile Countercurrent, *Geophys. Res. Lett.*, *22*, 211–214, 1995.

Strub, T. P., J. M. Mesias, V. Montecino, J. Rutllant, and S. Salinas, Coastal ocean circulation off western South America, in *The Sea*, edited by A. R. Robinson and K. H. Brink, pp. 273–313, John Wiley, New York, 1998.

Stuiver, M., and P. J. Reimer, Extended ^{14}C data base and revised CALIB 3.0 14C age calibration program, *Radiocarbon*, *35*(1), 215–230, 1993.

Stuiver, M., P. J. Reimer, E. Bard, J. W. Beck, G. S. Burr, K. A. Hughen, B. Kromer, G. McCormick, J. van der Plicht, and M. Spurk, INTCAL 98 radiocarbon age calibration, 24,000-0 cal B.P., *Radiocarbon*, *40*, 1041–1083, 1998.

Toggweiler, J. R., K. Dixon, and K. Bryan, Simulations of radiocarbon in a coarse-resolution world ocean model, 1, Steady state prebomb distributions, *J. Geophys. Res.*, *94*, 8217–8242, 1989.

Toggweiler, J. R., K. Dixon, and W. S. Broecker, The Peru upwelling and the ventilation of the South Pacific thermocline, *J. Geophys. Res.*, *96*, 20,467–20,497, 1991.

Wainer, I., and P. J. Webster, Monsoon/El Niño-Southern Oscillation relationships in a simple coupled ocean-atmosphere model, *J. Geophys. Res.*, *101*, 25,599–25,614, 1996.

Webster, P. J., and S. Yang, Monsoon and ENSO: Selectively interactive systems, *Q. J. R. Meteorol. Soc.*, *118*, 877–926, 1992.

Wooster, W. S., and J. L. Reid, Eastern boundary currents, in *The Sea*, edited by M. N. Hill, pp. 253–280, Nescience Publ., New York, 1963.

Wyrtki, K., Surface currents of the eastern tropical Pacific Ocean, *Inter-American Trop. Tuna Comm. Bull.*, *4*(5), 271–304, 1965.

Wyrtki, K., An estimate of equatorial upwelling in the Pacific, *J. Phys. Oceanogr.*, *11*, 1205–1214, 1981.

Yasunari, T., Impact of Indian monsoon on the coupled atmosphere/ocean system in the tropical Pacific, *Meteorol. Atmos. Phys.*, *44*, 29–41, 1990.

M. J. Feldberg and A. C. Mix, College of Oceanic and Atmospheric Sciences, Oregon State University, Corvallis, OR 97331, USA. (feldberg@smile.orst.edu)